RSC Advances

ROYAL SOCIETY OF CHEMISTRY

www.rsc.org/advances

GRAPHICAL ABSTRACT
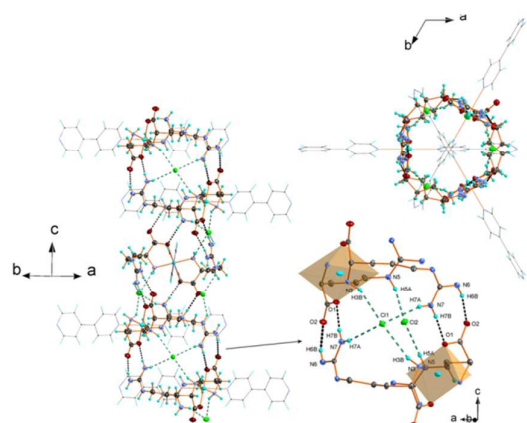
A novel 1D polymeric copper(II) complex, with L-arginine and a linear bridged 4,4′-bipyridine of a formula $\{[Cu(\text{L-Arg})_2(\mu\text{-}4,4'\text{-bpy})]Cl_2 \cdot 3H_2O\}_\infty$ (where L-Arg = L-argininie, 4,4′-bpy = 4,4′-bipyridine) was synthesized and its crystal structure and spectroscopic properties were characterized using X-ray diffraction, FT-IR, Raman, electron paramagnetic resonance (EPR) and NIR-vis-UV spectroscopy techniques as well as microbiological properties were analyzed.

Metal-organic framework in ʟ-arginine copper(II) ions polymer:

structure, properties, theoretical studies and microbiological

activity

Agnieszka Wojciechowska, [*a] Anna Gągor,[b] Wiktor Zierkiewicz,[a] Anna Jarząb,[c] Agnieszka Dylong[a] and Marek Duczmal[a]

[a]*Faculty of Chemistry, Wroclaw University of Technology, Wybrzeze Wyspiańskiego 27, 50-370 Wrocław, Poland*

[b]*Institute of Low Temperature and Structure Research, Polish Academy of Sciences in Wrocław, Okólna Street 2, 50-422 Wrocław, Poland*

[c]*Institute of Immunology and Experimental Therapy, Polish Academy of Sciences, R. Weigla Street 12, 53-114 Wrocław, Polanda*

* Corresponding author. Tel. +48 713203666; fax: +48 71 320 43 60. E-mail address:

agnieszka.wojciechowska@pwr.edu.pl (A. Wojciechowska).

Abstract A novel 1D polymeric copper(II) complex with L-arginine and a linear bridged 4,4′-bipyridine with a formula of $\{[Cu(L\text{-}Arg)_2(\mu\text{-}4,4'\text{-}bpy)]Cl_2 \cdot 3H_2O\}_\infty$ (**1**) (where L-Arg = L-argininie, 4,4′-bpy = 4,4′-bipyridine) was synthesized. The crystal structure and properties of product were characterized using X-ray diffraction, thermogravimetric analysis (TGA), differential scanning calorimetry (DSC), spectroscopic techniques (FT-IR, Raman, NIR-vis-UV electronic and EPR), magnetic methods, and microbiological examinations. The crystals of **1** crystallized in a trigonal system and space group of P 3_2 2 1 was characterized with a = 12.3060 Å, b = 12.3060 Å, c = 18.4537 Å, V = 2420.18 Å^3, Z = 3, α = β = 90° and γ = 120°. The N and O donor atoms of *trans*-chelated L-Arg zwitterions and two N atoms of 4,4′-bpy molecule form a tetragonal distorted octahedral geometry around copper(II) ions with static character (T = 0.748). The diffuse-reflectance electronic spectrum of **1** is characteristic of $[CuN_2N_2'O_2]$ chromophore. The EPR spectrum of frozen **1** (at 77 K) dissolved in water is related with N_2O_2 set ($g_\perp$ = 2.057, $g_{||}$ = 2,258 and $A_{||}$ = 169 G). The structure of $[Cu(L\text{-}Arg)_2(\mu\text{-}4,4'\text{-}bpy)]^{2+}$ model complex was optimized at the B3LYP and B3LYP-D3 levels. The calculations of the atomic spin densities on the atoms in the doublet state of the model complex revealed that, with regard to the ligands, the spin population is distributed mainly over the oxygen and nitrogen atoms of L-arginine. The antimicrobial activities were examined against the Gram-positive and -negative bacteria strains: *Streptococcus mutans, Enterococcus hirae*, *Bacillus subtilis*, *Staphylococcus aureus*, *Pseudomonas aeruginosa*, *Escherichia coli*, *Salmonella enterica, Shigella flexneri;* and fungi: *Saccharomyces cerevisiae, Candida albicans*. Complex **1** exhibited a strong antimicrobial activity against bacteria and fungi, both in their growth inhibition as well as in microbial killing.

Keywords: L-arginine, copper(II) complex, spectroscopic methods, DFT calculation, biological activity

1. Introduction

(S)-2-Amino-5-guanidinopentanoic acid, commonly known as L-arginine, has been used as a substance with nonlinear optical (NLO) characters in optoelectronics.[1] Most importantly, L-arginine is one of the basic amino acids encoded by DNA. In aqueous solutions, L-arginine appears as a zwitterion with protonated guanidine group, an spontaneous process resulting in a thermodynamically durable form in both solutions and crystals.[2–11] The presence of guanidine group in L-arginine is crucial for the structural similarity with two antibiotics—*netropsin* and *distamycin*. Both of these compounds are highly selective in binding with DNA regions rich in A-T pairs and are active anticancer and antiviral substances. Binding tightly to B-DNA, *distamycin* and *netropsin* penetrate minor groove and hinder the activity of polymerases. *Netropsin* inhibits the growth of gram-positive and gram-negative bacteria and the proliferation of animal viruses. *Distamycin* inhibits the synthesis of viral DNA *herpes simplex*. In addition, both antibiotics have *in vitro* and *in vivo* cytotoxic properties against *Ehrlich* and *Walker* tumors. Along with other compounds binding to the minor groove of DNA, they are used as DNA probes and DNA hybridization stabilizers. The modern carbocyclic analogues of both compounds have been widely studied for their anticancer activities.[12] It was also observed that *netropsin* forms chemical nucleases through binding with metal ions.[13] Similarly, L-arginine, revealing strong coordination properties, combines with metal ions to form crystalline complexes.[2–11] L-arginine and its metal ion complexes are considered as structural analogues of *distamycin* and *netropsin*. A particular analogue of *netropsin* in binding to AT-DNA are the complexes with formulas of [Cu(L-Arg)$_2$](NO$_3$)$_2$ and [Cu(L-Arg)(phen)Cl]Cl·2.5H$_2$O.[2,3] The studies involving a series of complexes of L-arginine and the ions of Cu^{2+} and VO^{2+} with heterocyclic ligands indicate that the binding efficiencies of these complexes with DNA is much greater than that

of pure L-arginine. The strongest binding between these complexes and DNA structure was observed for [Cu(L-Arg)(dppz)Cl]Cl and [Cu(L-Arg)$_2$](NO$_3$)$_2$, weaker binding for [Cu(L-Arg)(dpq)Cl]Cl and [Cu(L-Arg)(1,10-phen)Cl]Cl, and the weakest for [Cu(L-Arg)(bpy)Cl]Cl. A greater affinity for the formation of bonds with DNA occurs in the structures with an extended and flat heterocyclic ligand. It also seems interesting that strong binding of [Cu(L-Arg)$_2$](NO$_3$)$_2$, despite the lack of aromatic structure, is due to formation of a complex that fits complementarily into the shape of the major groove of DNA.[2,3]

Only three L-arginine hexa-coordinated metal(II) ions complexes have been studied to date. There are monomeric as well as two one-dimensional coordination polymers consist of metals ions, including [Co(L-Arg)$_2$(NO$_2$)$_2$]·NO$_3$·2H$_2$O, [Cu(L-Arg)$_2$]Hg$_2$Cl$_6$ and {[Cu$_2$(L-Arg)$_2$(2,2'-bpy)(µ$_2$-ClO$_4$)$_2$]·2ClO$_4$·4H$_2$O}$_n$.[14–16] Therefore, in the present paper, we describe in details the crystal structure of a novel one-dimensional copper(II) coordination polymer with a formula of {[Cu(L-Arg)$_2$(µ-4,4'-bpy)]Cl$_2$·3H$_2$O}$_\infty$ (**1**). The polymer framework was produced with bridged-organic ligand as 4,4'-bipyridine. A number of infinite frameworks built up from 4,4'-bpy groups have been reported in recent years due to their rod-like rigidity and length.[17–21]

The spectroscopic properties of title complex **1** in solid state as well as its aqueous solution (FT-IR, FT-Raman, NIR-vis-UV, EPR) were analyzed. Additionally, the structure of **1** was optimized; the values of interaction energies (ΔE) between each ligand and Cu^{2+} and the atomic spin density were calculated at the B3LYP-D3 level. The antimicrobial activity was examined against various microorganisms: *S. mutans*, *E. Hirae*, *B. subtilis*, *S. aureus*, *P. aeruginosa*, *E. coli*, *S. enterica*, *S. Flexneri*, *S. cerevisiae*, and *C. albicans.*

2. Results and discussion

Description of crystal structure of {[Cu(L-Arg)$_2$(µ-4,4'-bpy)]Cl$_2$·3H$_2$O}$_\infty$ (1)

{[Cu(L-Arg)$_2$(μ-4,4′-bpy)]Cl$_2$·3H$_2$O}$_∞$ (**1**) crystallizes in trigonal chiral structure with

P3$_2$21 space group. The unit cell accommodates three molecules of [Cu(L-Arg)$_2$(μ-4,4′-bpy)]$^{2+}$

complex with the metal at the center lying on the C$_2$ axis. In crystal structure of **1**, L-Arginine

exists as a single charged cation with a terminal protonated guanidinium [(H$_2$N)$_2$CNH]$^+$ and

deprotonated carboxylate COO$^-$ groups, therefore, additional Cl$^-$ ions as counter anion are

necessary to attain electroneutrality. The copper ion is coordinated by *trans*-chelating

carboxylate oxygen atoms (O1, O1′) and amine nitrogen atoms (N3, N3′) from two

equivalent L-Arg molecules and two nitrogen atoms (N1 and N2″) from two equivalent 4,4′-

bpy. Figure 1 illustrates the [Cu(L-Arg)$_2$(μ-4,4′-bpy)]$^{2+}$ complex with anisotropic displacement

parameters drown for symmetrically independent part.

The copper coordination sphere is a distorted octahedron of C$_2$ symmetry elongated

in [100] direction with shorter Cu−O1 and Cu−N3 bond distances of 1.933 and 1.917 Å in the

basal plane and longer Cu−N1 and Cu−N2 axial bonds of 2.523 and 2.695 Å, respectively.

Selected values of distances and angles are presented in Table 1.

The 4,4′-bpy rings are rotated about 32.8° (the C6−C4−C3−C2 torsion angle) probably

due to the cation-π interactions between the cationic L-Arg residue with aromatic chains of

4,4′-bpy. Two limiting geometries are possible for this kind of contacts: parallel configuration

of the planar guanidinium of L-Arg and the aromatic ring and perpendicular arrangement in

which the hydrogen atoms from NH$_2$ of the L-Arg point into the face of the aromatic ring.[22] In

the solid state, the stacking configuration dominates over the H-bonding arrangement;[23,24]

although, gas-phase calculations indicate that the perpendicular setting of a guanidinium-

benzene pair is more energetically favorable.[25] In {[Cu(L-Arg)$_2$(μ-4,4′-bpy)]Cl$_2$·3H$_2$O}$_∞$

complex, both configurations are present. The cationic L-Arg residue has a face-to-face

geometry with one 4,4′-bpy ring with C11−centroid distance of 3.980 (1) Å regardless of

$N6H_2$ group pointing towards the center of the second ring with N6–centroid distance of 3.801 (1) Å. Simultaneous presence of both geometries has been found in lactoferrin.[26]

Because 4,4′-bpy molecule coordinates to two different Cu^{2+} centers, the polymeric 1D structure is formed along the [100] direction (Fig. 2(a)). The separation distance between metal positions along the chain equals 12.306(1) Å. The dimers form layers in which they propagate in the same direction (Fig. 2(a)). Because of the 3_2 chiral axes along [001], the chains in adjacent layers are rotated by 120°, giving the packing illustrated in Fig. 2(b). The positive charge of $[Cu(\text{L-Arg})_2(\mu\text{-}4,4'\text{-bpy})]^{2+}$ is compensated by Cl^- ions that are statistically distributed in the crystal voids within three different accessible sites; forming numerous H bonds through L-Arg together with crystallized water. Cl1 atom serves as an acceptor in four H bonds with two N7–H groups of guanidine and two NH_2 groups joining two neighboring copper centers in c direction that are separated by 8.679 (1) Å. Cl2 atom interacts with N5H groups of L-Arg, also connecting two complexes. Additionally, H-bonded dimers of amino acid are formed through strong N7—H7B···O1^{iv} and N6—H6B···O2^{iv} hydrogen bonds. All these interactions constitute the crystal structure in c direction, forming H-bonded chiral channels. The details of the supramolecular structure are presented in Fig. 3 and Table 2. The crystallized water molecules in the crystal voids serve as acceptors for hydrogen from NH and NH_2 groups of L-Arg. These interactions are weak because the donor···acceptor (D—H···A) distances range from 3.28 (1) to 3.36 (1) Å.
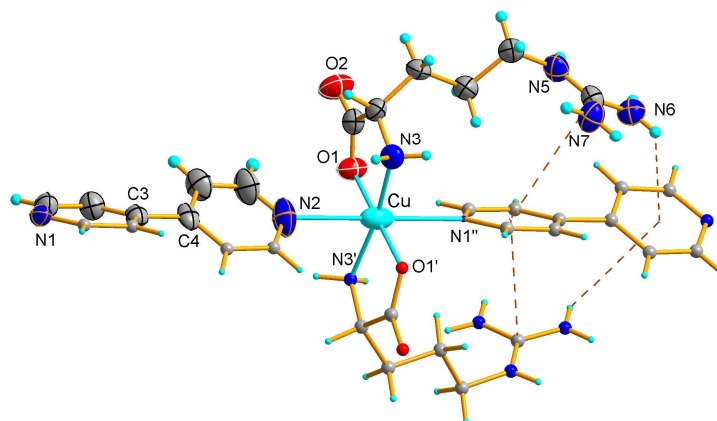
Fig. 1. Crystal structure of [Cu(L-Arg)$_2$(μ-4,4'-bpy)]$^{2+}$ complex. The asymmetric unit is presented in ellipsoid representation. Atoms involved in intermolecular bonding are labeled. Displacement ellipsoids are shown for atoms from asymmetric unit at 50% probability level. Dashed lines stand for cation-π interactions.

a)   b)
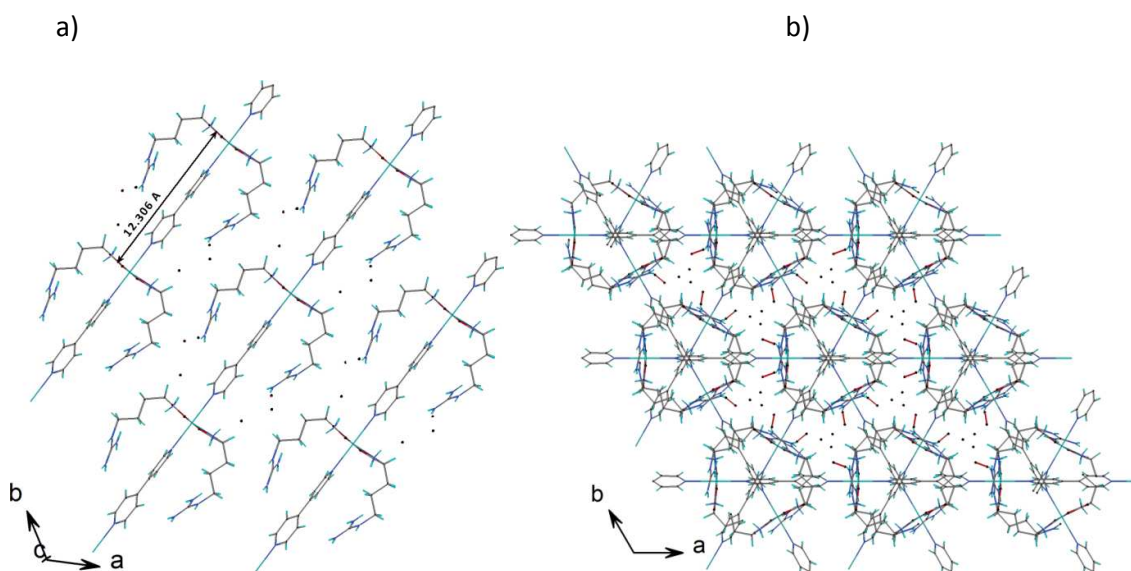
Fig. 2. (a) A layer of {[Cu(L-Arg)$_2$(μ-4,4'-bpy)]Cl$_2$·3H$_2$O}$_\infty$ dimmers; (b) packing diagram of **1** along the c-axis. Dots in the crystal voids stand for crystallized water and Cl3 ions.

Fig. 3. Supramolecular network in the structure of **1**; (a) H-bonded complexes viewed along c axis, (b) chiral molecular arrangement along the c direction, (c) enlarged motive with NH···O and NH···Cl hydrogen bonds.

Computational studies (DFT)

The structure of $[Cu(\text{L-Arg})_2(\mu\text{-}4,4'\text{-bpy})]^{2+}$ complex in aqueous solution optimized at B3LYP-D3 level is similar to that obtained in the experiment (Figs. 1 and 4). Complete geometry optimization of $[Cu(\text{L-Arg})_2(\mu\text{-}4,4'\text{-bpy})]^{2+}$ complex in aqueous solution, performed using the standard B3LYP method (without correction of the dispersion interactions), lead to a final structure significantly different from that obtained experimentally. In the B3LYP optimized structure, the L-arginine ligands are almost perpendicular to the plane passing

through the Cu, N1^{ii} and N2^{ii} atoms. The C11–N6–N2^{ii} and C11^{i}–N6^{i}–N2^{ii} angles can serve as a measure of L-arginine chain tilt. The experimental values of these angles are 151.26° and 151.25°, respectively. The B3LYP-D3 method underestimated these values related to the corresponding experimental X-ray data by 2.52° and 6.60°, whereas to the standard B3LYP method by 33.71° and 40.21°, respectively.
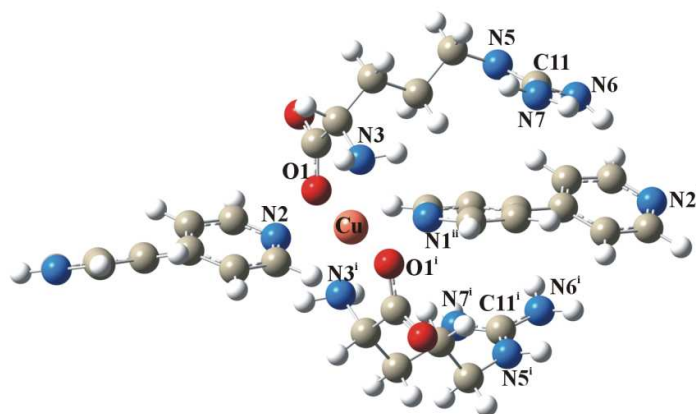

Fig. 4. Optimized structures of [Cu(L-Arg)$_2$(μ-4,4'-bpy)]$^{2+}$ complex in aqueous solution.

Table 1 lists the selected geometrical parameters calculated for the complex **1** and [Cu(L-Arg)$_2$(μ-4,4'-bpy)]$^{2+}$ model complex, indicating the differences between theoretical and experimental data. Some of the calculated bonds lengths and angles are overestimated whereas the others are–underestimated relative to the corresponding experimental X-ray data. For instance, the calculated N3–Cu, O1–Cu distances or the N3–Cu–N3, O1–Cu–N3 angles are larger than those in the experimental structure by: 0.084 Å, 0.045 Å; and 8.43°, 0.45°, respectively. On the other hand, when calculated using the B3LYP-D3 method, the bond lengths of N1–Cu and N2–Cu or angles of O1–Cu–O1 and N1–Cu–N2 were observed smaller than the experimental ones by 0.055 Å, 0.259 Å, and 3.06°, 1.04°, respectively.

For the optimized structure of $[Cu(L-Arg)_2(\mu-4,4'-bpy)]^{2+}$ cation complex, the interaction energies (ΔE) between each of the four molecules of ligands and the rest of the complex were calculated. The calculated ΔE of L-arginine ligands were −80.84 and −81.26 kcal mol^{-1} for the ligands situated at the top and bottom of the complex, respectively (Fig. 4). Whereas, the value of the interaction energy for 4,4'-bpy with N1^{ii} atom, located between two L-arginine ligands, was −18.58 kcal mol^{-1}. The ΔE value of the second 4,4'-bpy ligand was almost twice smaller, as −11.43 kcal mol^{-1}. This difference can be explained as a consequence of the interaction between two L-arginine ligands and one of the 4,4'-bpy ligands. Analogous results were obtained for $[Zn(L-Tyr)_2(\mu-4,4'-bpy)_2]$ complex, suggesting that the additional $\pi\cdots\pi$ stabilization interaction between L-tyrosine and 4,4'-bpy rings was responsible for the differences in ΔE values.[27] Therefore, in the case of $[Cu(L-Arg)_2(\mu-4,4'-bpy)]^{2+}$ complex, one can perhaps suppose that, the additional NH$\cdots\pi$ stabilizing interactions between L-arginine ligands and 4,4'-bpy rings are responsible for different values of ΔE. The complexes stabilized by the NH$\cdots\pi$ interactions between alanine and benzene ring have been reported.[28] It was demonstrated that in the case of NH$\cdots\pi$ stabilized alanine$\cdots$benzene unit, the B3LYP method failed for optimization of the geometry and prediction of the interaction energy value. It indicates that dispersion interaction neglected by B3LYP is very important for the stability of this complex. This could explain why the optimized structure at B3LYP and B3LYP-D3 levels are significantly different.

Table 3 lists the atomic spin densities (Δ) of selected atoms in the doublet state of $[Cu(L-Arg)_2(\mu-4,4'-bpy)]^{2+}$ complex calculated at the B3LYP-D3 level. The surface of the spin density for this complex is illustrated in Fig. 5. As these data reveal, most of the electron spin density is located on the metal center. The spin population on the copper atoms was found as 0.634e. Very similar value (0.628e) was obtained from the Mulliken population analysis.

The remaining spin population is distributed mainly over oxygen (O1, O1[i]) and nitrogen (N3, N3[i]) atoms of L-arginine ligands. Noteworthy, spin density on the N2 and N1[ii] atoms of 4,4'-bpy ligands are negligibly small (–0.001 e).
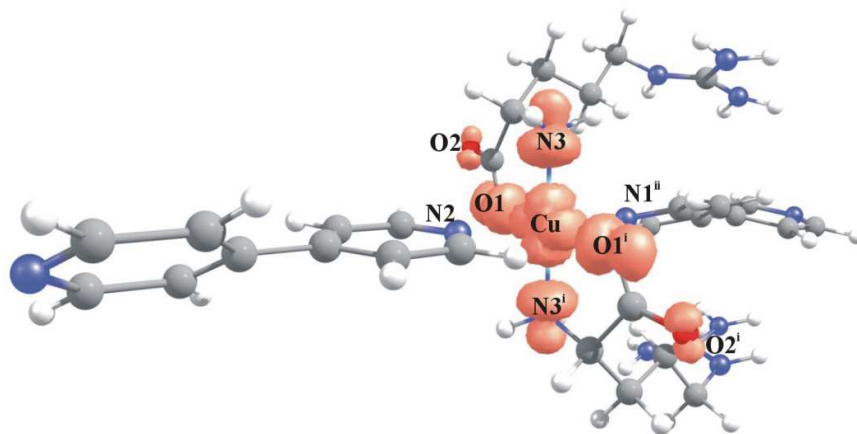

Fig. 5. Spin density isosurface (±0.002 au) calculated in doublet state of [Cu(L-arg)$_2$(μ-4,4'-bpy)]$^{2+}$ model complex.

Thermal stability

Thermal behavior of **1** was examined on the crystalline samples using TG-DTA and DSC techniques carried out under nitrogen and air atmosphere, respectively. The data of temperature ranges, mass losses, and thermal effects accompanying the decomposition are listed in Table 4 and presented in Figs. S2,3. The first stage of decomposition process occurred between 73 and 93 °C with 4.0% mass loss (calc. 3.9%), correlated to the loss of 1,5 crystal water molecules at 73 °C. Moreover, decomposition of 0.5 crystal water molecule was clearly observed at ~33 °C in the DSC thermogram but difficult to find in the TG-DTA thermogram. The almost anhydrous compound decomposed in several stages followed by several endo and exothermic effects. The endotherm at ~155 °C together with the mass loss of 12.8% (calc. 12.8%), is an evidence for the elimination of next water molecule and two chlorine anions. There was exothermic effect at 193 °C in the DTA thermogram due to the

loss of 4,4′-bpy molecule. The second exothermic stage took place between 249 and 331 °C

with 22.1% mass loss (calc. 25.1%), attributable to the L-arginine entity.

Vibrational and Raman spectroscopy

The comparison of FT-IR and Raman spectra and structural data provide

characteristic vibrations. In the spectral range of 3600–2800 cm^{-1}, the bands are generated

via stretching ν(C–H) vibrations of CH and CH$_2$ groups, ν(N–H) modes of NH and NH$_2$ in L–Arg

cations as well as stretching ν(O–H) vibrations (Figs. S4).[29] The spectrum of **1** exhibited

bands at 1683, 1660, 1631, 1597, and 1529 cm^{-1}. The weak and very strong absorptions at

1660, 1529, and 1597 cm^{-1} are related to the δ CH$_2$ vibrations, which are respectively well

related to the bands at 1651, 1529, and 1591 cm^{-1} observed in the spectrum of 4,4–bpy. The

energy region from 1750 to 1500 cm^{-1} is characteristic for out–of–plane bending of NH$_2$

group and ν_{as} (COO$^-$). The infrared bands observed at *ca.* 3500, 1700–1780, 1550–1610, and

1300–1420 cm^{-1} are characteristic for ν(–OH), ν(C=O), ν_{as}(COO$^-$), and ν_{sym}(COO$^-$) vibrations

of the carboxylate group, respectively.[29–33] These observations indicate very weak and other

strong bands in the vibrational spectrum for L–Arg at 1720 and 1552 cm^{-1}, caused by ν(C=O)

and ν_{as}(COO$^-$) vibrations. The ν(C=O) modes generated band at 1726 cm^{-1} in Raman spectra.

Unfortunately, in spectrum of complex **1**, the bands corresponding to ν(C=O) vibrations are

very difficult to observe in both IR and Raman spectra. But, the ν_{as}(COO$^-$) vibrations are

correlated to low–energetic component at *ca.* 1580 cm^{-1} of asymmetric band with maximum

at 1597 cm^{-1}. The ν_{sym}(COO$^-$) vibrations revealed relatively weak absorption below 1450 cm^{-}

^{1}. These modes produced the bands at 1419 cm^{-1} (L-Arg) and 1404 cm^{-1} (**1**) in IR spectrum.

Whereas, the Raman spectrum of L-Arg exhibits strong peaks at 1477, 1450, and 1437 cm^{-1},

which are assigned to δ CH$_2$, ν (C–N) and ν_{sym} (COO$^-$) vibrations, respectively. In Raman

spectrum of **1**, only one peak was observed at 1431 cm^{-1}, which could be correlated to ν_{sym}

of carboxylate group. The out–of–plane bending of NH_2 group is assigned to the strong

bands observed at 1676 and 1612, cm^{-1} for L–Arg and 1683 and 1631 cm^{-1} for complex **1**. It

is difficult to find the corresponding peaks in Raman spectra. In this region, the band

observed at 1601 cm^{-1} is in good agreement with the absorption band of 4,4′-bpy spectrum

at *ca.* 1606 cm^{-1}.

NIR-vis-UV electronic and EPR spectra

As shown in Fig. 1, the N and O atoms of *trans*-coordinated L-arginine zwitterions

together with t*rans*-N1 and N2 4,4′-bpy atoms produce elongated octahedral environment

around copper(II) ions (d^9 configuration) with chromophore $[CuN_2N_2'O_2]$. The N and O atoms

in amino acid are distanced *ca.* 1.952 Å. Whereas, the axial Cu–N1 and Cu–N2 bond lengths

are significantly different and are relatively long, equal to 2.523 and 2,695 Å, respectively,

resulted from Z-out distortion in octahedron. The difference of 0.163 Å is comparable with

0.164(6) Å, observed for $[Cu(2,2'-bpy)_3]^{2+}$ cations.[34] The distortion of copper(II) ion geometry

is usually described by tetragonality parameter, which tries to quantify whether a Jahn-Teller

distortion is ordered or disordered, and later it described the type of disordered as static or

dynamic.[34] The tetragonality is defined as the ratio of $T = d_{eq}/d_{ax}$. The d_{eq} is the average of

four equatorial bond distances, whereas d_{ax} is correlated with average of two axial bond

distances. When the value of T equals 1.0, the geometry distortion of copper(II) ions

presents dynamic character. The T values smaller than 0.9 are related to static geometry,

whereas they are diagnostic fluxional stereochemistry tool in the range of 1.0–0.9.[34] For **1**,

the T parameter with relatively low value of 0.748 suggest the static character of distortion

in $[Cu(L-Arg)_2(\mu-4,4'-bpy)]^{2+}$ complex. To date, the similar complexes of copper(II) ion built up

the *trans*-coordinated 4,4′-bpy molecules and chelated *N,O′* and *O,O′* molecules have been

structurally characterized in details: $\{[Cu(4,4'-bpy-bpy)(ccnm)_2]\cdot4MeOH\}$ (ccnm =

carbamoylcyanonitrosomethanide),[17] [Cu$_2$(benzoate)$_4$(4,4'-bpy)$_3$],[18] [Cu(PCPA)$_2$(4,4'-bpy)]$_n$

(PCPA = p-chlorophenoxyacetic acid),[19] [Cu(4,4'-bpy)(HCO$_3$)$_2$]$_n$,[20] and [Cu(L1)$_2$(4,4'-bpy)] (HL1

= 2-(2-metoxy phenylthio)benzoic acid)[21]. In these structures, the Cu–N$_{bpy}$ distances are in

the range of 1.988–2.0069 Å and are relatively shorter in comparison with Cu–O$_{carboxylate}$

(1.9322–2.643 Å) or Cu–N$_{ccnm}$ (2.707 Å) bonds.[17–21] It seems that the octahedral geometry

around copper(II) ions is strongly distorted with the oxygen atoms in the axial positions and

the values of T parameter vary between 0.988 and 0.746.[17–21] Unfortunately, the

spectroscopic characteristics using analysis of electronic spectroscopy was performed only

for [Cu(PCPA)$_2$(4,4'-bpy)]$_n$. The spectrum of this complex shows only a single band with

maximum at 17 300 cm^{-1} (578 nm, T = 0.828).[19] Whereas, the tetragonal with elongated

bonds on a z-axis geometry around Cu^{2+} ions in **1** produces a broad and splitted *d-d* band,

consisting of two relatively well separated components with maxima at 10 800 and 15 700

cm^{-1} (Fig. 6). The tetragonal field (D$_{4h}$) and the presence of Jahn-Teller effect splitted the ^{2}T$_{2g}$

into ^{2}Eg (d$_{xz}$, d$_{yz}$) and ^{2}B$_{2g}$ (d$_{xy}$), and ^{2}E$_g$ levels into ^{2}A$_{1g}$ (d$_{z2}$) and ^{2}B$_{1g}$ (d$_{x2-y2}$) components.

Therefore, the expected three transitions should occur from highly destabilized *d$_{x2-y2}$* orbital

^{2}B$_{1g}$ state to ^{2}A$_{1g}$, ^{2}B$_{2g}$, and ^{2}E$_g$ states. Further, in crystal field of D$_{2h}$ symmetry, the ^{2}T$_{2g}$ and

^{2}E$_g$ levels can be divided into B$_{1g}$ (d$_{xy}$), B$_{2g}$ (d$_{xz}$), and B$_{3g}$ (d$_{yz}$), and into A$_{1g}$ (d$_{x2-y2}$) and A$_{1g}$ (d$_{z2}$),

respectively.[35,36] The analysis based on the filtration process revealed the presence of four

components as it was expected for D$_{2h}$ symmetry. The maximum at 10 800 cm^{-1} splits at

8740 and 10 440 cm^{-1}, whereas the second band at 15 700 cm^{-1} consists of two components

at 14 100 and 16 010 cm^{-1} (Fig. 6), resulting from A$_{1g}$ (d$_{x2-y2}$) → A$_{1g}$ (d$_{z2}$), B$_{3g}$ (d$_{yz}$) B$_{2g}$ (d$_{xz}$), and

B$_{1g}$ (d$_{xy}$) transitions.
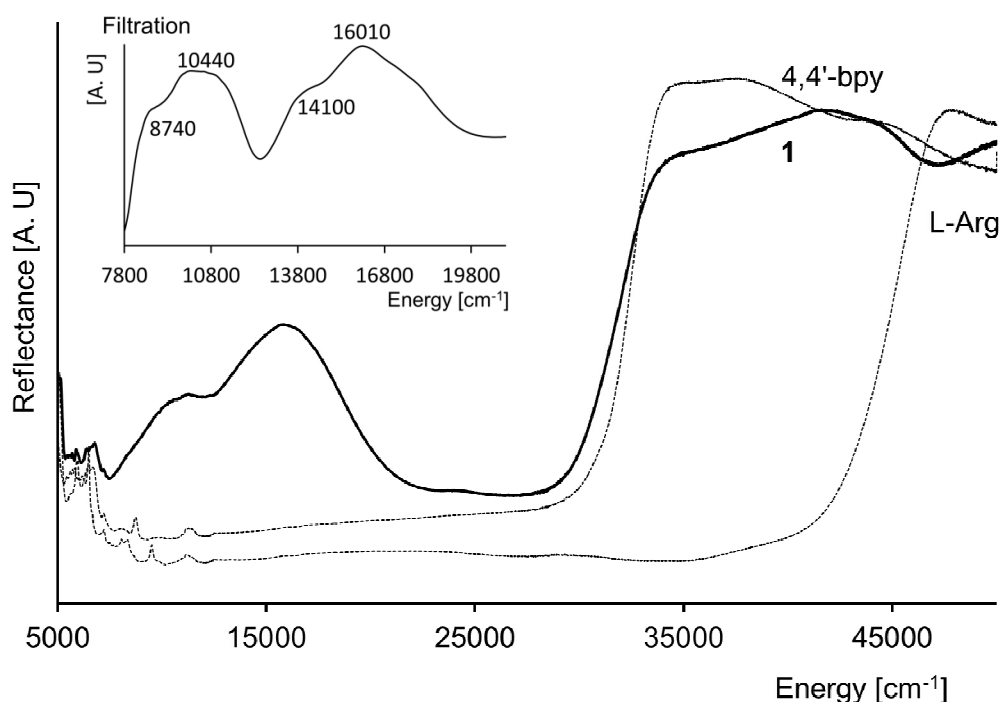
Fig. 6. The diffuse-reflectance spectra of $\{[Cu(L\text{-}Arg)_2(\mu\text{-}4,4'\text{-}bpy)]Cl_2 \cdot 3H_2O\}_\infty$ (**1**) and ligands and the effect of filtration process of *d-d* band (filter parameters: step = 20 cm^{-1}, α = 200 and N = 60).

The EPR spectra of powder recorded with X-bands at 293 and 77 K corresponds to S = 1/2 state of Cu(II) ion in coordination sphere of elongated axial symmetry. The spin Hamiltonian parameters are slightly temperature dependent, $g_\perp$ = 2.067 and $g_{||}$ = 2.201 at 293 K, and $g_\perp$ = 2.072 and $g_{||}$ = 2.223 at 77 K. The relation of $g_{||} \gg g_\perp > 2.0023$ is in agreement with $d_{x2\text{-}y2}$ orbital of unpaired electron ground state.

Magnetic measurements

The magnetic susceptibility of **1** (Fig. 7) shows the Curie–Weiss behavior in the whole temperature range with a Weiss constant θ of 0.10 K and a magnetic moment of 1.81 μ_B. The effective magnetic moment slightly decrease below 5 K to 1.79 μ_B at 1.8 K. Crystals of **1** are composed of layers in which the copper ions in each layer are arranged in the chains bridged by 4,4'-bpy molecules (Fig. 2). The neighboring chains are connected through very

long bridges containing NH···O hydrogen bonds: Cu-N3-C7-C8-C9-C10-N5-C11-N7-H7B···O1-Cu. Such a long contact mediated by ten atoms suggests that any interchain exchange interactions are negligible. Taking into account the structural features, the magnetic susceptibility data were fitted using a high-temperature series expansion (HTSE) derived from the one dimensional Heisenberg model for $S = \frac{1}{2}$, based on the Padé approximation technique[37,38]:

$$\chi = (Ng^2\beta^2 / 4kT) [N/D]^{2/3}$$

in which $N = 1.0 + 5.7979916y + 16.902653y^2 + 29.376885y^3 + 29.832959y^4 + 14.036918y^5$,

$D = 1.0+2.7979916y + 7.0086780y^2 + 8.6538644y^3 + 4.5743114y^4$, and $y = J/4kT$ (adjusting the equation to $H = -JS_1S_2$ convention). A good agreement between the simulated and experimental susceptibility was achieved with $J = -0.043$ cm^{-1}, and $g = 2.091$ (very close to the average EPR value of 2.113), R = $\Sigma[(\chi T)_{exp} - (\chi T)_{calc}]^2 / \Sigma[(\chi T)_{exp}]^2 = 1.2\cdot10^{-5}$ (66 points).

Complexes in which the 4,4'-bpy molecule serves as a bridging ligand are relatively rare. The most likely reason is that after the formation of M–N bond by one of the nitrogen atoms, the second atom is protonated or participates in hydrogen bonding, which limits its coordination ability.[39] Despite the small number of examples, it appears that the angle between the two rings of 4,4'-bpy molecule plays the key role in transmission of magnetic exchange interactions. For [Cu$_2$(dien)$_2$(4,4'-bpy)(ClO$_4$)$_2$](ClO$_4$)$_2$ (dien = diethylenetriamine), where the rings are coplanar, the exchange integral has been determined as -0.9 cm^{-1}, although the authors failed to exclude the contribution of interdimer interactions.[39] On the other hand, for [Cu(4,4-bpy)$_3$(DMSO)$_2$](ClO$_4$)$_2$·2(4,4'-bpy), with a very large angle (61.4°), no interactions were detected down to 2 K.[40,41] In the case of the intermediate angle between the pyridyl rings (28.02°), found in [Cu$_2$(mal)$_2$(H$_2$O)$_2$(4,4-bpy)] (H$_2$mal = malonic acid), the parameter of exchange through the bridging 4,4'-bpy was estimated at -0.052 cm^{-1}.[42] It follows that the magnitude of the exchange parameter in **1** ($J = -0.043$ cm^{-1}, the angle

between the rings 32.8°) is very small, but consistent with the coupling constants measured

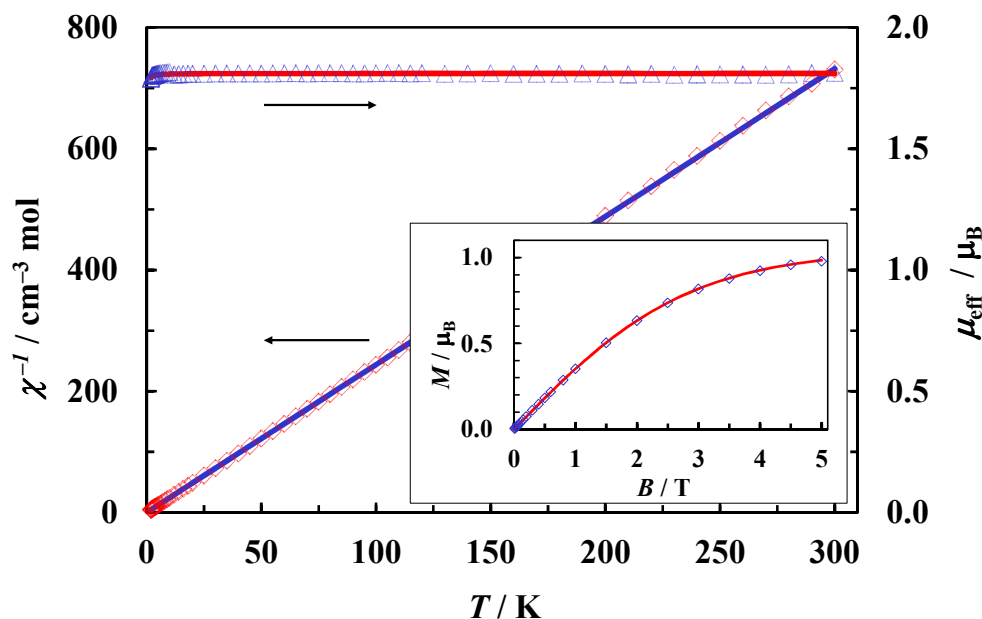for other similar 4,4'-bpy bridged copper(II) complexes.

Fig. 7. Plots of reciprocal magnetic susceptibility χ^{-1} (◇) and effective magnetic moment μ_{eff}

(Δ) versus temperature for **1**. The solid lines correspond to the best fit parameters (see text).

Inset: Magnetization as a function of magnetic induction at 2.00 K. The line is the Brillouin

function calculated for S = ½, g = 2.091.

Solutions

NIR-vis electronic and EPR spectra

The absorbance spectrum of complex **1** solution in water was observed completely

different from the spectra in the solid state. However, this spectrum stayed in well

agreement with spectrum measured after 30 days, indicating that the coordination sphere is

unchanged upon the dissolution. It is very important in the context of biological studies for

substances prepared in solution. These spectra present only one very broad, intense, and

symmetric *d-d* band with a maximum at 16 100 cm^{-1} (Fig. 8). But, importantly, this spectrum

is comparable with the spectra observed for aqueous mixture of CuCl$_2$ (**2**) or CuSO$_4$ (**3**) and L-arginine in molar ratio 1 : 2, forming [Cu(L-Arg)$_2$]$^{2+}$ complex in solution. Additionally, the maximum of *d-d* band obtained for absorbance spectrum of aqueous/methanol mixture of CuSO$_4$: L-Arg : 4,4'-bpy (**4**) in molar ratio of 1 : 2 : 1 was *ca.* 16 200 cm^{-1}. These four spectra have great similarities (Fig. 8), enabling a comparison between spectrum of **1**, (**2**), (**3**), and (**4**) that suggests the presence of [Cu(L-Arg)$_2$]$^{2+}$ complex in the compound **1** solution in water. The observation indicates crashing of Cu−N1^{ii} and Cu−N2 coordination bounds in solution. It may exist, because the calculated values of interaction energy for L-arginine and 4,4'-bpy are significantly different and the molecule of heterocyclic amine makes weaker bond with copper(II) ions (ΔE *ca.* −80 and −15 kcal mol^{-1} for L-Arg and 4,4'-bpy, respectively).
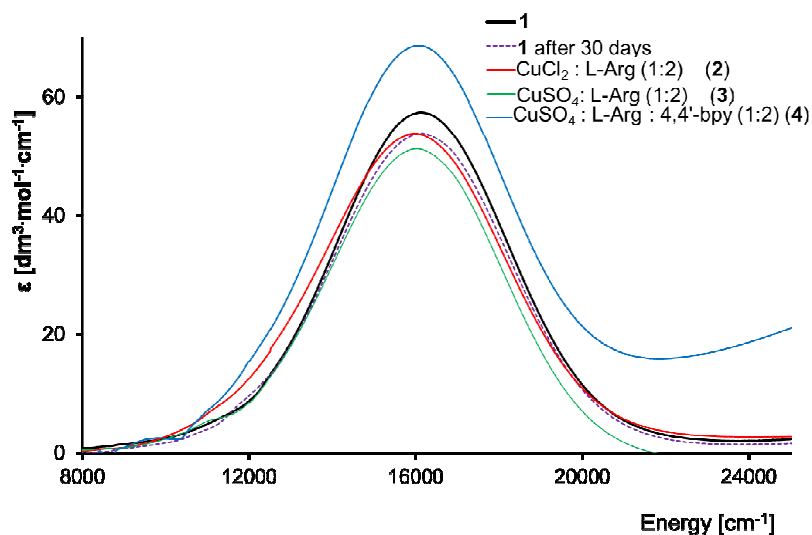
Fig. 8. Absorbance spectra of: **1** dissolved in H$_2$O and recorded after 30 days; mixtures of Cu^{2+} : L-Arg (**2**, **3**) and Cu^{2+} : L-Arg : 4,4'-bpy (**4**).

The spectrum of frozen aqueous solution of complex **1** is typical for monomeric species and exhibits hyperfine splitting (HFS) around g$_{||}$ due to the presence of copper nuclei (I = $^3/_2$) (Fig. 9(a)). The diagonal components of g tensor, obtained through simulation of the experimental spectrum, g$_\perp$ = 2.057, g$_{||}$ = 2258, and A$_{||}$ = 169 G reveal the square planar N$_2$O$_2$

chromophore around copper(II) ions in *xy* plane. The g- and A- tensor diagonal components

are very close to the parameters found for the spectrum of frozen mixture (**2**) (Fig. S5(b)).

The line at magnetic field of 3300 G also split further into five components, arising from the

hyperfine interactions with two equivalent ^{14}N nuclei (I = 1) of amino group NH_2.[43] The

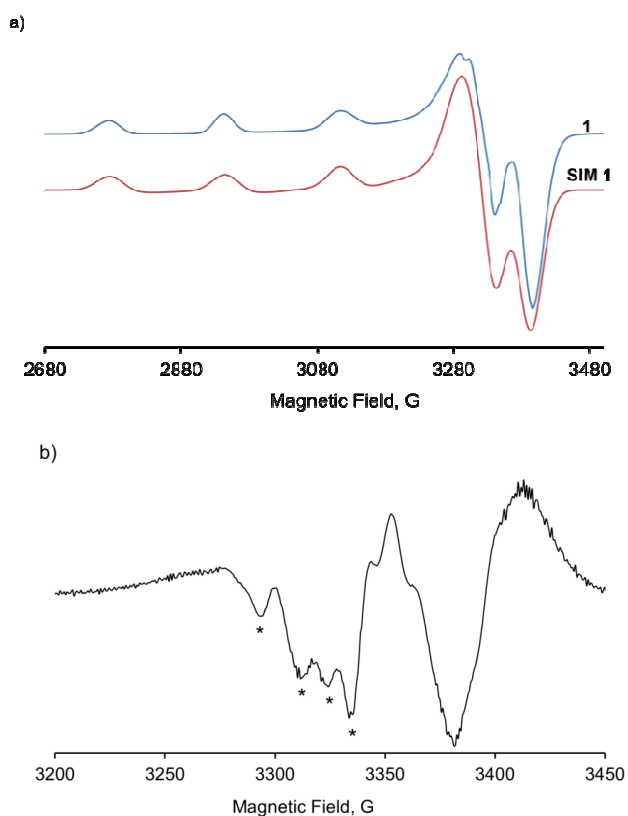second derivative of this line indicates the hyperfine splitting pattern (Fig. 9(b)).

Fig. 9. EPR spectra of frozen aqueous solution of: (a) complex **1** together with the spectra

simulated using the spin Hamiltonian parameters given in the text, (b) the second derivative

of line at about 3300 G.

Antibacterial and antifungal activities

The earlier studies indicate that L-arginine may influence the microbial susceptibility. This amino acid can increase the sensitivity of *P. aeruginosa* to two commonly used antibiotics of ciprofloxacin and tobramycin in mature biofilms. It was demonstrated that antibiotics administrated with L-Arg showed 10 to 100 fold greater activity in biofilm reduction than antibiotics administrated alone, which may be associated with the ability of L-arginine to increase the metabolic rate of the bacteria remaining in the lower levels of biofilm, especially in anoxic conditions.[44] Another study [45-46] also demonstrated the L-Arg antimicrobial properties realized through affecting their metabolic pathways. The chitosan-arginine (Ch-Arg) complexes reduce *E. coli* O157 growth in lag or exponential phase.[45] Chitosan is a carbohydrate extracted from shellfish commonly used as an antimicrobial agent and food preservative. Chemical derivatives of chitosan with positively charged L-arginine may increase the surface charge density, thus, the Ch-Arg complex reveals greater antimicrobial effect against Gram-negative bacteria than unmodified chitosan.[46] Similar studies indicated the antibacterial activity of the Cu-L-Arg complex against *S. aureus*, *S. pyogenes*, and *E. coli*.[47] They suggested L-Arg as an important agent that can increase the antimicrobial susceptibility to many drugs and antimicrobial agents while it does not influence the microbial killing alone. It seems that L-arginine and its combination with other compounds are commonly used as antiviral, antibacterial, and anticancer agents, which has an crescent-shaped molecular structures and selectively bind to the AT-rich sequence of DNA. After effective binding to DNA, *netropsin* and *distamycin* avoid interacting with DNA and proteins involved in the regulation of replication and transcription.[2,3] Inhibition of these crucial processes may have an indirect influence on the microbial growth and their sensitivities to various antimicrobials.

The results of the antimicrobial susceptibility examinations of **1** with four gram-positive, four gram-negative, and two fungal strains are presented in Fig. 10. All the ten examined strains were sensitive to the solution of $\{[Cu(\text{L-Arg})_2(\mu\text{-}4,4'\text{-bpy})]Cl_2 \cdot 3H_2O\}_\infty$ (**1**) (MIC < 15 M). The growth of gram-positive strains was inhibited after 24 h incubation with complex **1** in standard MIC test. The MABA test also revealed antimicrobial activity of **1**, especially to *S. mutans* with very high sensitivity. Whereas, the activities of **1** against gram–negative strains, *P. aeruginosa* and *S. enterica Typhimurium*, have been attributed at least to its high concentration. Compound **1** was observed to have inhibitory antibacterial activity against *E. coli* and *S. flexneri* at concentrations smaller than 8 μM. On the other hand, complex **1** manifested antifungal activity against the opportunistic pathogen *C. albicans* and also exhibited activity against *S. cerevisiae*. In addition, it should be noted that *P. aeruginosa*, *C. albicans*, and *S. cerevisiae* grow very quickly. However, a strong antimicrobial activity against those strains was observed for **1**, both in their growth inhibition (MIC testing) as well as in microbial killing (MABA testing). It can be noted that L-arginine may facilitate transportation of antimicrobial components, such as 4,4'-bpy, into pathogen calls, which may increase the microbial sensitivity to this complex.[48] But, the most important thing is the cationic guanidinium terminal group in L-Arg molecule, which can act as an effective photosynthesizer and model of DNA minor grove-binding molecule such as antibiotics *netropsin* and *distamycin*.

We also performed studies on the reference compounds, which are involved in **1**. The complex **1** demonstrated better activities against most of the examined microbes than 4,4'-bpy, the standard antimicrobial agent (Figs. S6,7). This observation may be associated with the biological activity of molecules coordination complexes.[49] Coordination ions increase lipophilic character of compounds and enhance the ability to permeate the cell membrane of

microorganisms. These features of coordination ions have been also suggested as reasons for their improved activity over their parent ligands. Chelation can reduce the polarity of the metal ion through partial sharing of its positive charge with the donor group of active compound and have greater affinity to microbial membrane.[50] Promising antimicrobial activities of some amino acids, such as arginine and glutamic acid with metal ions chelates, have been reported.[51]
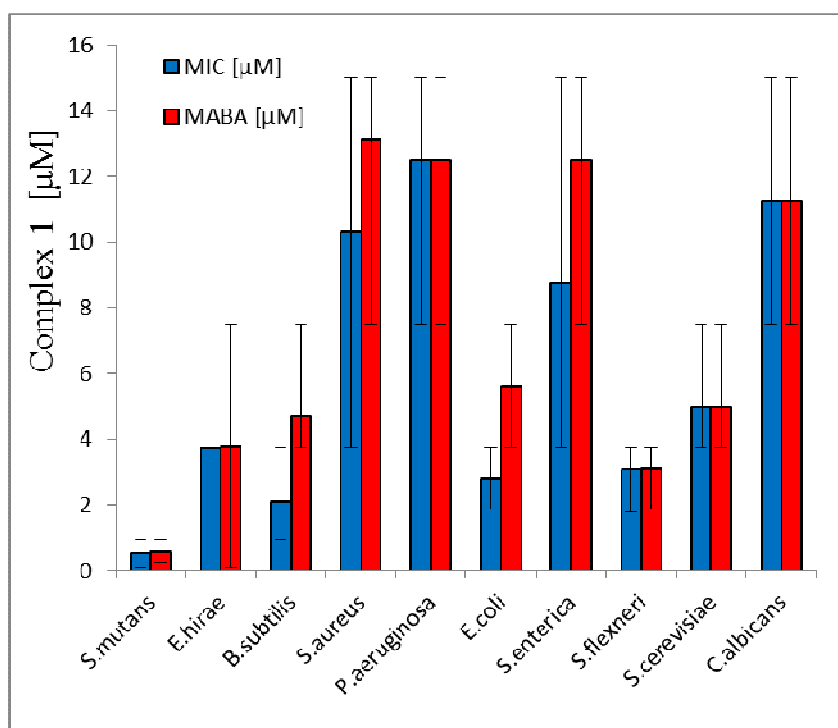
Fig. 10. Antimicrobial activities of dissolved {[Cu(L-Arg)$_2$(μ-4,4'-bpy)]Cl$_2$·3H$_2$O}$_\infty$ (**1**) complex in gram-positive and gram-negative bacteria and fungi measured through standard MIC and MABA examinations.

3. Conclusions

In conclusion, we accomplished the first L-arginine metal ions complex with metal-organic framework in crystals of {[Cu(L-Arg)$_2$(μ-4,4'-bpy)]Cl$_2$·3H$_2$O}$_\infty$ (**1**). The structural elongated octahedral coordination geometry is supported by diffuse-reflectance electronic spectra. The most interesting point is the behavior of **1** in aqueous solution. The absorbance

NIR-vis-UV electronic spectra of **1** dissolved in H_2O and mixture of Cu^{2+}:L-Arg: 4,4′-bpy (**4**) as well as theirs EPR spectra indicated four coordinated Cu^{2+} ions with N_2O_2 chromophore. It is directly connected with cracking of $Cu-N_{by}$ bonds in solvent. This observation was supported by theoretical studies on the nature of titled complex. The calculated (DFT) interaction energies (ΔE) for 4,4′-bpy were only −18.58 and −11.43 kcal mol^{-1}, whereas the L-arginine zwitterions are strongly bonded with copper centre (ΔE = −80.84 and −81.26 kcal·mol^{-1}). In addition, it was observed that $\{[Cu(L-Arg)_2(\mu-4,4'-bpy)]Cl_2 \cdot 3H_2O\}_\infty$ (**1**) aqueous solution possesses antimicrobial activity against bacteria and fungi.

4. Experimental

Copper(II) chloride, L-arginine, and 4,4′-bipyridine were purchased from Sigma-Aldrich. All reagents were used without further purification. Gram-positive bacteria (*S. aureus* PCM 2054, *B. subtilis* PCM 2021, *S. mutans* PCM 2502, and *E. hirae* PCM 2559), gram-negative bacteria (*Pseudomonas aeruginosa* PCM 2058, *Escherichia coli* PCM 1144, *S. enterica Typhimurium* PCM 2565, and *S. flexneri* PCM 1793) and fungi (*C. albicans* PCM 2566 and *S. cerevisiae* PCM 2567) were obtained from the Polish Collection of Microorganisms (PCM) of the Institute of Immunology and Experimental Therapy, Polish Academy of Sciences (Wroclaw, Poland). The Alamar Blue colorimetric indicator assay was purchased from Bio-Rad.

*Synthesis of complex **1***

$\{[Cu(L-Arg)_2(\mu-4,4'-bpy)]Cl_2 \cdot 3H_2O\}_\infty$ (**1**). Complex **1** was prepared directly through reaction between the ligands and Cu(II) chloride. An aqueous solution of $CuCl_2 \cdot 2H_2O$ (5 mL, 0.1 M) was slowly added into an aqueous solution of L-arginine (10 mL, 0.1 M) and methanol solution of 4,4′-bpy (5 mL, 0.1 M) under moderate stirring. The solution was allowed to

slowly evaporate at room temperature and crystallize 4,4′-bpy in 14 days. The crystals of 4,4′-bpy were then filtered and the resulting clear mixture was kept at room temperature to slowly dry. After 25 days, blue crystals of complex **1** were obtained. Anal. Calcd for $C_{22}H_{42}N_{10}O_7Cl_2Cu$ (FW = 693,1 g/mol): C, 38.12; H, 6.10; N, 20.21; Cl, 10.23; Cu, 9.17. Found: C, 37.91; H, 6.26; N, 19.95; Cl, 10.32; Cu, 8.76. All values are given as percentage.

X-ray structural analysis and refinement

       The crystal structure of **1** was determined from single-crystal X-ray diffraction data. The diffraction intensities were collected on an Xcalibur diffractometer operating in κ-geometry, equipped with a two-dimensional CCD detector. *Mo Kα* radiation (0.71073 Å) was used. Acquisition was performed in ω-scan mode with $\Delta\omega = 1.0°$ using CrysAlis CCD program. The CrysAlis RED software version 1.170.32 (Oxford Diffraction)[52] was used for data processing. Empirical absorption correction was applied using spherical harmonics, implemented in SCALE3 ABSPACK scaling algorithm. The structure was solved through direct methods and was refined using the full-matrix least–squares method against F^2 with SHELX–97 program package.[53] Anisotropic displacement parameters were applied for all non-hydrogen atoms. The hydrogen atoms not involved in H-bond interactions were produced geometrically (C–H 0.96 Å) and treated as riding atoms. Disordered solvent H_2O molecules were located from the difference Fourier maps on three positions with occupancies of: 0.27, 0.73, and 0.5 for O_{w1}, O_{w2}, and O_{w3}, respectively. Additionally, the O_{w3} site was interchangeably occupied with chlorine Cl3 with site occupation factor of 0.2. The H atoms from disordered molecules were not identified. The details of the crystal data and data collection and refinement are presented in Table S1. X-ray diffraction data of powders were collected in a reflection mode, in the Bragg–Brentano geometry using X'Pert PRO X-ray diffraction system. Fig. S1 presents XRD patterns for **1** . The diffractogram is consistent with

powder diagram calculated for the crystal structure found from the single-crystal x-ray diffraction. Obtained powders were homogenous without the traces of additional phases. The differences in relative intensity for some peaks are originated from the texture effects.

Computational studies (DFT)

The DFT calculations were performed for $[Cu(\text{L-Arg})_2(\mu\text{-4,4'-bpy})]^{2+}$ complex. This complex is an open-shell system in which the calculated ground electronic state is doublet. In the optimization procedure, the fragment of the crystallographic structure of the title compound was used as the starting geometry. The calculations were performed using B3LYP-D3 method (standard hybrid density functional B3LYP[54,55] method corrected with the original D3 damping function).[56] The following combined basis sets were used in the calculations: LanL2DZ [57] for Cu atom in conjunction with the D95V(d,p) [58] basis set for all atoms of the ligands. For all of the optimized structures of complexes, vibrational frequencies were calculated to verify whether the optimized molecular structures corresponded to minimum energy. All calculations were performed for complexes in aqueous solutions using the polarizable continuum model (PCM).[59a] The interaction energy between selected ligand and the rest of the complex was calculated as a difference between electronic energies of the whole complex and a sum of the energies of the selected ligand and the rest of the complex. The value of the BSSE correction to the interaction energy (for the complex in solvent) was estimated based on the calculated contribution of this correction to the interaction energy (for the complex in gas phase) calculated using the counterpoise method.[59b] Atomic spin densities were calculated through a natural bond orbital (NBO) analysis applied separately to α and β spin density matrices, as described by Carpenter and Weinhold.[60–62] All computations were carried out with Gaussian 09 set of programs.[63]

Spectroscopic, thermal and magnetic examinations

ATR FT-IR spectra of complex **1**, L-Arg, and 4,4'-bpy spectra were collected using a Bruker Vertex 70 v Fourier transform infrared spectrophotometer equipped with a diamond attenuated-total-reflection infrared cell. The spectra were measured with 4 cm^{-1} resolution in the ranges of 4000–400 and 600–50 cm^{-1} at room temperature. Instrument control and initial data processing were performed using OPUS program (v. 7.0 Bruker Optics, Ettlingen, Germany). The FT-Raman spectra of **1** and ligands were obtained on a Bruker MuliRam spectrometer (Nd:YAG laser with a liquid radiation at wavelength of 1064 nm) equipped with a liquid N_2 cooled germanium detector. The spectra were measured at conditions of: resolution 2 cm^{-1}, co-addition of 256 scans, and laser power values of 1 (for **1**) and 150 mW (for L-Arg and 4,4'-bpy).

The NIR–vis–UV electronic spectra were obtained on a Cary 500 Scan Spectrophotometer over the range 5000–50 000 cm^{-1} with a measure step of 10 cm^{-1} at 293 K. Diffuse solid-state reflectance spectra were measured for **1**, L-Arg, and 4,4'-bpy with identical parameters as a baseline of white reference sample. Absorbance spectra were recorded for solutions of **1** and L-Arg in H_2O and 4,4'-bpy in methanol with concentrations of 1.4×10^{-2}, 2.0×10^{-3}, and 0.1×10^{-3} M, respectively. Additionally, the absorbance spectra of mixture consisting of aqueous solution of $CuCl_2$ (**2**) or $CuSO_4$ (**3**) and L-Arg in molar ration 1:2 and mixture consisting of aqueous solutions of $CuSO_4$ and L-Arg, and methanol solution of 4,4'-bpy in molar ration 1:2:1 (**4**) were recorded ($c_{cu2+} = 3.33 \times 10^{-2}$ M). To obtain the bands positions, the variable digital filtering analysis was applied.[64–66] The reflectance spectrum of **1** was filtered with the filter parameters of: α = 200, N = 60 and step = 20.

EPR spectra were measured using a Bruker Elexys E 500 spectrometer equipped with NMR teslameter (ER 036TM) and frequency counter (E 41 FRC) at X-band of solid state and

frozen solution at 77 K of complex **1** dissolved in H_2O. The aqueous mixture of **3** and **4** were also collected at room and 77 K temperatures. The experimental spectra were simulated using computer program, DoubletExact (S = 1/2) written by Andrew Ozarowski from NHMFL, University of Florida.

Thermogravimetric analysis (TG-DTA) was carried out using a Setaram SETSYS 16/18 system, operating under nitrogen atmosphere with a heating rate of 5 °C min^{-1} in the range of 30–500 °C (sample mass 10.392 mg). Differential scanning calorimetry (DSC) examinations were performed on a Setaram DSC 92 instrument. Sample (mass 10.4 mg) was contained in aluminum pan in presence of air as the furnace atmosphere with heating rate of 5 °C min^{-1} in the range of 25–500 °C.

The magnetic susceptibility of complex 1 in the temperature range of 1.8–300 K in a magnetic field strength of 500 mT and magnetization up to 5 T were measured with a Quantum Design SQUID magnetometer. The diamagnetic corrections (-363×10^{-6} emu mol^{-1}) were applied on the calculated results using Pascal's constants.

Antimicrobial susceptibility testing

The standard MIC (minimal inhibitory concentration) test was performed according to Clinical and Laboratory Standards Institute (CLSI) method.[67] Bacteria and fungi were grown from an overnight agar culture of the test organisms. Inoculum for the MIC test was prepared through taking three to five well-isolated colonies of the same morphology from an agar plate culture. The top of each colony was touched with a sterile loop and the growth was transferred into a tube containing 10 mL of sugar enriched broth. The broth culture was incubated overnight at 37 °C while shaking. The turbidity of the actively growing broth culture was adjusted with sterile broth to obtain turbidity comparable to that of the 0.5 McFarland standards to obtain a suspension containing approximately 1×10^8 to 2×10^8

cfu/mL. Inocula (100 µL) were incubated on 96-well plates containing 100 µL of **1** at various concentrations (0.12–15 µM) dissolved in sugar broth and the control row with 100 µL of sugar broth without antimicrobial agent at 37 °C for overnight. The optical density of each well was read at 600 nm in a plate reader (BioTek). The MIC represents the concentration of antimicrobial at which there was complete inhibition of growth and was taken as the lowest concentration of the tested antimicrobial agent that shows no visible bacterial growth. To determine whether dissolved complex **1** affects the microbial killing, all wells were examined with the microwell alamar blue assay (MABA),[68] an indirect susceptibility assay by adding 20 µL of an indicator Alamar Blue (Bio-Rad). The plates were then re-incubated for 2 h at 37 °C and the fluorescence was read for each well. The cellular growth and viability were determined. This sensitive oxidation-reduction dye becomes blue and non-fluorescent, when cells are dead or pink and fluorescent upon reduction by live cells to its oxidized form. Cell growth was determined through fluorescence measurement on Perkin Elmer EnSpire 2300 Multilabel Reader (Waltham, MA, USA) and visual color change. All testing procedures were repeated 5 times in duplicates.

Table 1 Selected bond distances (Å) and angles (deg) in complex **1**

Distances	Exper.	Theor. [a,b]	Angles	Exper.	Theor. [a,b]
Cu1—O1[i]	1.933 (3)	1.981 (0.048)	O1[i]—Cu1—N3[i]	95.28 (15)	95.75 (0.45)
Cu1—N3[i]	1.971 (4)	2.055 (0.084)	O1[i]—Cu1—N3	84.74 (14)	84.57 (−0.18)
Cu1—N3	1.971 (4)	2.055 (0.084)	N3[i]—Cu1—N3	170.6 (2)	179.07 (8.43)
Cu1—N1[ii]	2.523 (6)	2.468 (−0.055)	O1–Cu–O1	179.6 (1)	176.7 (−3.06)
Cu1—N2	2.694 (7)	2.436 (−0.259)	O1–Cu–N3[i]	95.3 (2)	95.23 (−0.03)
C11—N5	1.309 (6)	1.338 (0.029)	O1–Cu–N3	84.7 (2)	84.51 (−0.22)
C11—N6	1.320 (6)	1.347 (0.027)	N1[ii]–Cu–N2	180.0	178.96 (−1.04)
C11—N7	1.315 (6)	1.343 (0.029)	–	–	–

Symmetry code: (i) *x-y*, *-y*, *-z*+1/3; (ii) 1+x, y,z [a] Results from the B3LYP-D3 calculations for the model complex (Fig. 4). [b] Differences between theoretical and experimental data are given in parenthesis.

Table 2 Hydrogen bond interactions in the crystal structure of complex **1**

D—H···A	D—H	H···A	D···A	D—H···A
N3—H3A···Cl3[ii]	0.90	2.08	2.941 (6)	160
N3—H3B···Cl1[iii]	0.90	2.64	3.450 (4)	151
N7—H7A···Cl1[iii]	0.86	2.51	3.245 (5)	144
N7—H7B···O1[iv]	0.86	2.00	2.857 (6)	174
N6—H6A···O2W	0.86	2.46	3.288 (7)	162
N6—H6A···O1W	0.86	2.48	3.279 (12)	155
N6—H6B···O2[iv]	0.86	2.09	2.937 (6)	167
N5—H5A···Cl2[v]	0.86	2.39	3.097 (5)	140
N5—H5A···O1W	0.86	2.57	3.362 (12)	154
N5—H5A···O1W[vi]	0.86	2.63	3.346 (12)	142

Symmetry codes: (ii) y, x−1, -z; (iii) x, y−1, z; (iv) y+1, x−1, -z; (v) −x+y+1, −x, z+1/3; (vi) −x+2, −x+y+1, −z+2/3.

Table 3 NBO and Mulliken atomic spin density [Δ, in e] on selected atoms in the doublet state of the [Cu(L-Arg)$_2$(μ-4,4′-bpy)]$^{2+}$ complex. Calculation performed at the B3LYP-D3 level.

	α	β	$\Delta^{a,b}$
Cu1	14.122	13.488	0.634 (0.628)
O1	4.479	4.391	0.088 (0.088)
O2	4.389	4.376	0.013 (0.013)
N3	4.030	3.941	0.089 (0.091)
O1^{i}	4.479	4.392	0.087 (0.087)
O2^{i}	4.388	4.375	0.013 (0.013)
N3^{i}	4.029	3.939	0.090 (0.092)
N2	3.799	3.800	−0.001 (−0.001)
N1^{ii}	3.796	3.797	−0.001 (−0.001)

[a] Spin density calculated as difference between values of α and β. [b] Mulliken atomic spin densities are given in parentheses.

Table 4 Summary of TG-DTA and DSC analyses data of (**1**).

Stage	$T^*_{deh,i}$ (°C)	T^*_{max} (°C)	$\Delta H°$ $(J\,g^{-1})^{**}$	Weight loss (%)	Evolved moiety formula	Mass calc. (%)
1.	73	93	119.9	4.0	1.5 H_2O	3.9
2.	155	162	71.1	12.8	1.0 H_2O + 2Cl$^-$	12.8
3.	193	210	−16.4	22.1	4,4'-bpy	22.5
4.	249	276	−17.2	−	−	−
5.	329	331	−56.8	22.1	L-Arg	25.1

*Experiments carried out under nitrogen atmosphere; **experiments carried out in presence of air as the furnace atmosphere;

Acknowledgments

Appendix A. Supplementary data

Crystallographic data for the structure reported in this paper have been deposited with Cambridge Crystallographic Data Center. Copies of this information are available free of charge on request, quoting the following deposition CCDC number: 1042998, from The Director, CCDC, 12 Union Road, Cambridge, CB2 1EZ, UK, fax: +441 223 336 033, e-mail: deposit@ccdc.cam.ac.uk or the website: http//www.ccdc.cam.ac.uk.

References

1   (*a*) F. Machado, L. Souhesa, R. Cunha, F. Cabral, A. Rodrigues, J. Carvalho and R. Santana, *J. Phys. Chem. Solid,* 2010, **71***,* 862; (*b*) A. Pragasam, S. Selvakumar, K. Thamizharasan, D. Anand and P. Sagayaraj, *J. Cryst. Growth,* 2005, **280**, 271; (*c*) T. Prasanyaa, M. Haris, V. Jayaramakrishnan, M. Amgalan and V. Mathivanan, *Physica Scripta,* 2013, **88**, 045403.

2   A. K. Patra, T. Bhowmick, S. Ramakumar and A. R. Chakravarty, *Inorg. Chem.,* 2007, **46***,* 9030.

3   A. K. Patra, T. Bhowmick, S. Roy, S. Ramakumar and A. R. Chakravarty, *Inorg. Chem.,* 2009, **48***,* 2932.

4   P. Sasmal, R. Majumdar, R. Dighe and A. Chakravarty, *Dalton Trans*. 2010, **39**, 7104.

5   S. Liao, X. Le, X. Feng, *J. Coord. Chem.,* 2008, **61**, 847.

6   A. Alagha, D. Brown, M. Elawad, H. Muller-Bunz, H. Nimir, A. Yanovsky and K. Nolan, *Inorg. Chim. Acta,* 2011, **377**, 185.

7   R. Hu, Q. Yu, F. Liang, L. Ma, X. Chen, M. Zhang, H. Liang and K. Yu, *J. Coord. Chem.,* 2008, **61**, 1265.

8   H. Hemissi, M. Nasri, S. Abid, S. Al-Deyab, E. Dhahri, E. Hlil and M. Rzaigui, *J. Solid State Chem.,* 2012, **196**, 489.

9   P. Bacarea, I. Neda, C. Daniliuc, A. Bacarea and L. Dimitrescu, *Rev. Chim.,* 2012, **63**, 489.

10 P. Arularsan, B. Sivakumar, G. Chakkaravarthi and R. Mohan, *Acta Cryst.,* 2013, **E69**, m583.

11 T. Yajima, G. Maccarrone, M. Takani, A. Contino, G. Arena, R. Takamido, M. Hanai, Y. Funahashi, A. Odani and O. Yamauchi, *Chem. Eur. J.,* 2003, **9**, 3341.

12 (*a*) D. Drozdowska and J. Szerszenowicz, *Lett. Drug Des. Discov.,* 2012, **9,** 12; (*b*) D. Drozdowska, *Molecules,* 2011, **16**, 3066; (*c*) D. Drozdowska, M. Rusak, W. Miltyk and K. Midura-Nowaczek, *Archiv der Pharmazie–Chem. Life Sciences,* 2009, **342**, 87.

13 C. Bailly and J. B. Chaires, *Bioconjugate Chem.,* 1998, **9**, 513.

14 W. Watson, D. Johnson, M. Celap and B. Kamberi, *Inorg. Chim. Acta*, 1972, **6**, 591.

15 M. Zabel, V. Pavlovskii and A. L. Poznyak, *J. Struct. Chem*., 2008, **49**, 758.

16 X. Zhou, C. Yang, X. Le, S. Chen, J. Liu and Z. Huang, *J. Coord. Chem*., 2004, **57**, 401.

17 A. S. R. Chesman, D. R. Turner, G. B. Deacon and S. R. Batten, *Chem. Commun*., 2010, **46**, 4899.

18 S.-T. Wu, L.-S. Long, R.-B. Huang and L.-S. Zheng, *Crystal. Growth Des*., 2007, **7**, 1746.

19 Y. Sun, Z. Wang, H. Zhang, Y. Cao, S. Zhang, Y. Chen, Ch. Huang and X. Yu, *Inorg. Chim. Acta*, 2007, **360**, 2565.

20 H.-X. Guo, X.-Z. Li, Ch.-X. Chen, L. Zheng, *J. Chem. Crystallogr.,* 2010, **40**, 564.

21 L. Lu, W. Jun, Z. Feng-Chun, W. Wei-Ping, Z. Xiu-Lan and X. Bin, *Synth. React. Inorg. Metal-Organic, nano-Metal Chem*., 2013, **43**, 1319.

22 J. C. Ma and D. A. Dougherty, *Chem. Rev.*, 1997, **97**, 1303.

23 T. R. Knochel, M. Hennig, A. Merz, B. Darimont, K. Kirschner and J. N. Jansonius, *J. Mol. Biol.,* 1996, **262**, 502.

24 H. Kurokawa, B. Mikami and M. Hirose, *J. Mol. Biol.,* 1995, **254**, 196.

25 E. M. Duffy, P. J. Kowalczyk and W. L. Jorgensen, *J. Am. Chem. Soc.,* 1993, **115**, 9271.

26 M. Haridas, B. F. Anderson and E. N. Baker, *Acta Crystallogr.,* 1995, **D51**, 629.

27 A. Wojciechowska, J. Janczak, W. Zierkiewicz, A. Dylong and E. Matczak-Jon, *Polyhedron,* 2014, **85**, 665.

28   N. Mohan, K. P. Vijayalakshmi, N. Koga and C. H. Suresh, *J. Comput. Chem.,* 2010, **31**,

      2874.

29   S. Kumar and S. B. Rai, *Indian J. Pure Appl. Phys.,* 2010, **48**, 251.

30   A. M. Petrosyan and R. P. Sukiasyan, *J. Mol. Struct.,* 2008, **874**, 51.

31   A. M. Petrosyan, *Vibrat. Spectr.,* 2006, **41**, 97.

32   I. Viera, M. H. Torre, O. E. Piro, E. E. Castellano and E. J. Baran, *J. Inorg. Biochem.,* 2005,

      99, 1250.

33   Z. H. Sun, L. Zhang, D. Xu, X. Q. Wang, X. J. Liu, G. H. Zhang, *Spectrochim. Acta, Part A*,

      2008, **71**, 663.

34   B. Murphy, M. Aljabri, M. A. Aaleya, G. Murphy, B. J. Hathaway, M. E. Light, T. Geilbrich

      and M. B. Hursthouse, *Dalton Trans*., 2006, **2**, 357.

35   A. B. P. Lever, Inorganic Electronic Spectroscopy, Elsevier, New York, NY, USA, 1984.

36   S. N. Bolotin, E. L. Isaeva, M. H. Shamsutdinova, K. S. Pushkareva and N. N. Bukov, *Adv.*

      Phys. Chem., 2009, **2009** 365949.

37   G. A. Baker, Jr., G. S. Rushbrooke and H. E. Gilbert, *Phys. Rev.,* 1964, **135**, A1272.

38   O. Kahn, *Molecular Magnetism*, VCH Publishers, Inc., New York, 1993.

39   M. Julve, M. Verdauger, J. Faus, F. Tinti, J. Moratal, Á. Monge and E. Gutiérrez-Puebla,

      Inorg. Chem., 1987, **26**, 3520.

40   J. D. Woodward, R. Backov, K. A. Abboud, H. Ohnuki, M. W. Meisel and D. R. Talham,

      Polyhedron, 2003, **22**, 2821.

41   J. D. Woodward, Chemical and physical characterization of hybrid organic/inorganic

      low-dimensional coordination polymers, PhD thesis, University of Florida, Gainesville,

      2002

42   Y. Rodríguez-Martín, C. Ruiz-Pérez, J. Sanchiz, F. Lloret and M. Julve, *Inorg. Chim. Acta*,

2001, **318**, 159.

43   (*a*) N. Ohata, H. Masuda and O. Yamauchi, *Inorg. Chim. Acta,* 1999, **286**, 37; (*b*) S.

Dhanuskodi, P. A. Angeli Mary and P. Sambasiva Rao, *Spectrochim. Acta, Part A,* 2005,

61, 721.

44   G. Borriello, L. Richards, G. D. Ehrlich and P. S. Stewart, *Antimicrob. Agents Chemother.,*

2006, **50**, 382.

45   R. A. Lahmer, D. L. Jones, S. Townsend, S. Baker and A. P. Williams, *Int. J. Food Sci.*

Tech., 2014, **49**, 515.

46   R. A. Lahmer, A. P. Williams, S. Townsend, S. Baker and D. L. Jones, *Food Control,* 2012,

26, 206.

47   M. S. Iqbal, S. J. Khurshid and M. Z. Iqbal, *J. Pak. Med. Assoc.,* 1990, **40**, 221.

48   M. C. Grenier, R. W. Davis, K. L. Wilson-Henjum, J. E. LaDow, J. W. Black, K. L. Caran, K.

Seifert and K. P. Minbiole, *Bioorg. Med. Chem. Lett.,* 2012, **22**, 4055.

49   T. O. Aiyelabola, I. A. Ojo, A. C. Adebajo, G. O. Ogunlusi, O. Oyetunji, E. O. Akinkunmi

and A. O. Adeoye, *Adv. Biol. Chem.,* 2012, **2**, 268.

50   E. L. Chang, C. Simmers and D. A. Knight, *Pharmaceuticals,* 2010, **3,** 1711.

51   A. Legler, A. Kazachenko, V. Kazbanov, O. Per'yanova and O. F. Veselova, *Pharma.*

Chem. J., 2001, **35**, 501.

52   CrysAlisCCD CrysAlis RED, Oxford Diffraction Ltd., Version 1.171.33.42, release 29-05-

2009 CrysAlis171, **2009**.

53   G. M. Sheldrick, *Acta Cryst.,* 2008, **A64**, 112.

54   A. D. Becke, *J. Chem. Phys.,* 1993, 5648.

55   C. Lee, W. Yang and R. G. Parr, *Phys. Rev. Part B,* 1988, **37**, 785.

56   S. Grimme, J. Antony, S. Ehrlich and H. Krieg, *J. Chem. Phys.,* 2010, **132**, 154104.

57   P. J. Hay and W. R. Wadt, *J. Chem. Phys.,* 1985, **82**, 299.

58   T. H. Dunning Jr. and P. J. Hay, in Modern Theoretical Chemistry, Ed. H. F. Schaefer III,
      Vol. 3 (Plenum, New York, 1976) 1.

59   (*a*) J. Tomasi, B. Mennucci and R. Cammi, *Chem. Rev.,* 2005, **105**, 2999; (*b*) S. F. Boys
      and F. Bernardi, *Mol*. *Phys*.*,* 1970, **19**, 553.

60   A. E. Reed, L. A. Curtiss and F. Weinhold, *Chem. Rev.,* 1988, **88**, 899.

61   E. D. Glendening, A. E. Reed, J. E. Carpenter, F. Weinhold, NBO 3.1 Theoretical
      Chemistry Institute, University of Wisconsin, Madison, WI, 1996.

62   J. E. Carpenter and F. Weinhold, *J. Mol. Struct. (Theochem),* 1988, **169**, 41.

63   M. J. Frisch, G. W. Trucks, H. B. Schlegel, G. E. Scuseria, M. A. Robb, J. R. Cheeseman, G.
      Scalmani, V. Barone, B. Mennucci, G. A. Petersson, H. Nakatsuji, M. Caricato, X. Li, H.P.
      Hratchian, A. F. Izmaylov, J. Bloino, G. Zheng, J. L. Sonnenberg, M. Hada, M. Ehara, K.
      Toyota, R. Fukuda, J. Hasegawa, M. Ishida, T. Nakajima, Y. Honda, O. Kitao, H. Nakai, T.
      Vreven, J.A. Montgomery, Jr., J.E. Peralta, F. Ogliaro, M. Bearpark, J. J. Heyd, E.
      Brothers, K. N. Kudin, V.N. Staroverov, R. Kobayashi, J. Normand, K. Raghavachari, A.
      Rendell, J.C. Burant, S. S. Iyengar, J. Tomasi, M. Cossi, N. Rega, J. M. Millam, M. Klene,
      J. E. Knox, J.B. Cross, V. Bakken, C. Adamo, J. Jaramillo, R. Gomperts, R. E. Stratmann,
      O. Yazyev, A. J. Austin, R. Cammi, C. Pomelli, J. W. Ochterski, R. L. Martin, K.
      Morokuma, V. G. Zakrzewski, G. A. Voth, P. Salvador, J. J. Dannenberg, S. Dapprich, A.
      D. Daniels, O. Farkas, J. B. Foresman, J. V. Ortiz, J. Cioslowski, D. J. Fox, Gaussian, Inc.,
      Wallingford CT, 2009.

64   G. Bierman and H. Ziegler, *Anal. Chem.,* 1986, **58**, 536.

65   J. Myrczek, *Spectr. Lett.,* 1990, **23**, 1027.

66   A. Wojciechowska, W. Bronowska, A. Pietraszko, Z. Staszak and M. Cieślak-Golonka, *J. Mol. Struct.,* 2002, **608**, 151.

67   Clinical and Laboratory Standards Institute (CLSI). Reference Method for Broth Dilution Antifungal Susceptibility Testing of Yeasts; Approved Standard-Third Edition. CLSI document M27-A3 (ISBN 1-56238-666-2). Clinical and Laboratory Standards Institute, 940 West Valley Road, Suite 1400, Wayne, Pennsylvania 19087-1898 USA, 2008.

68   (*a*) G. Li, L. L. Lian, L. Wan, J. Zhang, X. Zhao, Y. Jiang, L. L. Zhao, H. Liu and K. Wan, *PLoS One*, 2013, **8**, e84065; (*b*) S. N. Rampersad, Sensors (Basel) 2012, **12**, 12347.